Online Supplement

"When Shared Autonomous Electric Vehicles Meet Microgrids: Citywide Energy-Mobility Orchestration"

Appendix A: Data Summary

Table 5 Data List

Categories	Data sets	Data sources
Energy	City-level electricity consumption by sector	New York State Energy Research and Development Authority (NYSERDA 2018)
	City-level electricity consumption by hour	NYISO (2018)
	Hourly residential, commercial and industrial load pattern	Office of Energy Efficiency & Renewable Energy (EERE 2014)
	Hourly solar radiation intensity	NREL (2014)
Transportation	Records of green and yellow taxi trips	TLC (2017)
	Vehicle related data (battery capacity, charge and discharge rate, charge and discharge conversion efficiency)	Battery University (2018), Clipper Creek (2018)
Geographic information	Geographical distribution of buildings at zip-code level	Department of City Planning (2018)
	Parking spots	Bursa (2014)

Table 6 City-Level Descriptive Statistics

	Mean	Standard deviation	Min	Max
7am-6pm				
Taxi trips ($\times 10^3$ hr^{-1})	35.68	2.62	31.81	40.60
Electricity consumption (MW)	9,121	451	8,146	9,585
Solar power generation potential (MW, 30% adoption level)	9,861	3,598	3,647	14,207
6pm-7am				
Taxi trips ($\times 10^3$ hr^{-1})	27.18	17.09	5.61	47.11
Electricity consumption (MW)	7,402	911	6,351	8,803
Solar power generation potential (MW, 30% adoption level)	484	1,047	0	3,615

Table 7 Microgrid-Area-Level Descriptive Statistics

Microgrid area ID	1	2	3	4	5	6	7	8	9	10
Num. of zip-code areas	9	10	11	7	3	8	7	9	5	11
Local solar utilization (%, whole day)	100	100	100	100	100	94.53	87.41	99.80	80.94	85.08
Microgrid area ID	11	12	13	14	15	16	17	18	19	20
Num. of zip-code areas	16	9	13	8	4	11	10	5	8	4
Local solar utilization (%, whole day)	99.96	78.41	97.43	78.08	89.98	81.63	81.67	93.22	68.37	73.14

Appendix B: Estimating Zip-Code Level Electricity Loads

We estimate the hourly electricity load profiles (and then interpolate the estimates of the loads of 15-min periods) of the 168 zip-code areas that span NYC (any zip-code area that is encircled by another zip-code area is combined into the encircling area). The main idea of estimation is to decompose the city-level electricity consumption data (which is available for each sector and each hour) into zip-code level estimates, while ensuring the consistency with other known information such as sector-specific load patterns and the weights of each load pattern at each zip-code area.

More specifically, for each zip-code area $k \in K = \{1, 2, ..., 168\}$ and hour of the day $t \in T = \{1, 2, ..., 24\}$, we denote the electricity consumption by $\hat{\phi}_{kt}$. To estimate $\hat{\phi}_{kt}$, we break it down into three load-specific parts. Mathematically, let $\hat{\phi}_{kt} = \sum_{p \in P} \phi_{ktp}$, where $P = \{1, 2, 3\}$ is the set of commercial, residential and industrial sectors, and ϕ_{ktp} represents the electricity consumption by sector p during hour t. We assume that the main pattern of load variation ϕ_{ktp} over a day is captured by a given sector-specific pattern f_{tp}. In other words, we model ϕ_{ktp} as $(\theta_{kp} + \epsilon_{ktp}) \cdot f_{tp}$, where θ_{kp} is a scale factor and ϵ_{ktp} represents hourly specific deviations off the pattern. The rationale of using fixed load patterns f_{tp} as regression bases is that the load variations exhibit strong similarities within each sector (e.g., commercial loads plateau around 7am-6pm and subside at other hours), which we observe from the OpenEI energy usage data sets (EERE 2014). These data sets include extensive records of hourly electricity consumption profiles of various load types across the United States. We choose the data sets of NYC to obtain f_{tp}. Then we formulate the following quadratic program to estimate ϕ_{ktp}:

$$\min_{\phi, \theta, \epsilon} \sum_{k \in K} \sum_{t \in T} \sum_{p \in P} \epsilon_{ktp}^2 \tag{20}$$

$$\text{s.t.} \quad \phi_{ktp} = (\theta_{kp} + \epsilon_{ktp}) \cdot f_{tp}, \quad \forall k \in K, t \in T, p \in P, \tag{21}$$

$$\sum_{k \in K} \sum_{p \in P} \phi_{ktp} = u_t, \quad \forall t \in T, \tag{22}$$

$$\sum_{k \in K} \sum_{t \in T} \phi_{ktp} = y_p, \quad \forall p \in P, \tag{23}$$

$$\theta_{kp} = \sum_{t \in T} \frac{\phi_{ktp}}{24 f_{tp}}, \quad \forall k \in K, p \in P, \tag{24}$$

$$\frac{\phi_{ktp}}{c_{kp}} = \frac{\sum_{k \in K} \phi_{ktp}}{\sum_{k \in K} c_{kp}}, \quad \forall k \in K, t \in T, p \in P, \tag{25}$$

$$\phi_{ktp}, \theta_{kp} \geq 0, \quad \forall k \in K, t \in T, p \in P. \tag{26}$$

In the above formulation, the objective (20) is to minimize the sum of the squared deviations so that the estimates ϕ_{ktp} are consistent with the known patterns. Constraints (21) define the electricity consumption with sector-specific load patterns and deviations. Constraints (22) ensure that the sum of electricity consumption by zip-code areas and by sectors is equal to the total electricity consumption of the entire city (u_t), which we obtained from New York Independent System Operations (NYISO 2018). Constraints (23) utilize the information of the electricity consumption breakdown by sectors (NYSERDA 2018). In NYC, the commercial sector accounts for 52% of electricity consumption, followed by the residential and industrial sectors that account for 34% and 14% of electricity consumption, respectively. Constraints (24) determine the average scale factor for each zip-code-by-sector category as the ratio of electricity consumption to the consumption amount in the pattern basis. Constraints (25) impose the assumption that, for each zip-code area k, the load of each sector is proportional to the building floor area c_{kp} of this sector, which was collected from the Department of City Planning (2018). Finally, constraints (26) impose non-negativity of the electricity consumption and scale factors.

The above formulation in the form of quadratic programme can be efficiently solved and can output solutions ϕ_{ktp}, which yields $\hat{\phi}_{kt}$ as the estimates of the zip-code level electricity load profiles.

Appendix C: Additional Data Sourcing and Processing

Delimiting microgrid areas: After estimating electricity load profiles, we next partition NYC into 20 microgrid areas using a standard k-means algorithm. Figures 3(a) and 3(c) show the load profiles and the layout of these areas. Such delimitation of microgrid areas eases computation and illustration, yet still allowing us to capture heterogeneities in mobility demands, load consumption and PV generation across different

areas. The detailed number of zip-code areas that each microgrid area clusters is summarized in Table 7 in Appendix A. Our findings are numerically tested to be valid for alternative clustering methods that consider the similarity or complementarity of load profiles within each area. The actual delimitation of microgrids areas would depend on various socio-technical complexities that are difficult to foresee and are not the focus of this work.

PV power output: The PV power generation potential (before any curtailment) in each period for each area is equal to the product of solar radiation intensity in that period, the installation area of PV panels and the conversion rate of PV panels. The data of solar radiation intensity is available online from the National Renewable Energy Laboratory (NREL 2014). To set the installation area of PV panels, we collect the data of the geographical distribution of buildings at the zip-code level from the Department of City Planning (2018). Each of the 847,998 records contains the information regarding the building floor area, the number of floors, zip-code and land use in detail. We calculate the rooftop area based on the building floor area and the number of floors. Since not all the rooftops are suitable for installing PV panels, we set the adoption level $\lambda = 30\%$ to represent a paradigm of solar-powered microgrids (lower and higher adoption levels are examined in Subsection 5.6. Finally, we set the conversion rate of PV panels at 40% (Ward 2017). As shown in Table 6 in Appendix A, the maximum solar power generation potential during 7am-6pm (14,207 MW) can also be regarded as the solar capacity. This approximation is validated by the alternative formula (Solar capacity = Total PV power generation in a day ÷ Average number of peak sun hours) according to 8MSolar (2016). Figure 3(b) shows the hourly PV power generation potential of ten microgrid areas. Figures 3(a)-(c) collectively show that, in general, central commercial districts such as Areas 1, 2 in Downtown and Midtown Manhattan have relatively high electricity demand yet inadequate local PV power generation due to the rooftop space limit. In contrast, as presented in Table 7 in Appendix A, most of other areas are residential and have excess PV power generation that cannot be locally utilized.

Microgrid interconnection and stationary energy storage: Microgrids are connected to the main grid and can be interconnected to exchange energy. However, the reverse power injection out of a microgrid due to excess local PV power generation may cause problems such as over-voltage on distribution feeders and increased short-circuit currents. As Pepco (2020) suggests, the actual reverse flow limit hinges on an array of power systems engineering factors. For simplicity, we set the reverse flow capacity factor at $\kappa = 30\%$, and will examine the impact of perturbing this value in the next subsection. Moreover, we assume that microgrids

are colocated with lithium-ion batteries, which represent the most popular technology for distributed energy storage systems (Pickerel 2020). In line with the energy storage goals of NYC, we set the total power capacity of energy storage at $\sum_i \bar{h}_i = 1$ GW as the baseline value for 15-minute time period (NYSDPS 2018), and allocate this capacity to each microgrid in proportion to the ratio of the local PV power generation to the local load, that is, $\bar{h}_i = \sum_i \bar{h}_i \times \left(\frac{\sum_t g_{it}}{\sum_t l_{it}} \Big/ \sum_i \frac{\sum_t g_{it}}{\sum_t l_{it}} \right)$. According to NYSDPS (2018), we assume that energy storage devices can discharge at full capacity for five consecutive hours, which translates to a total energy capacity of the stationary storage devices of $\sum_i \bar{s}_i = 5$ GWh. Finally, we set the charge and discharge efficiencies of energy storage at $\hat{\eta} = 90\%$ (Zablocki 2019).

Ride-share trip demands: We estimate ride-share trip demands in each period based on the records of yellow and green taxis from the NYC Taxi & Limousine Commission (TLC 2017). The public data set contains trip-level pick-up and drop-off times, locations and trip distances. We group the records to the zip-code level by matching trip origins and destinations to their zip-code areas, and then calculate the average taxi trip demands of each period for the 20 clustered microgrid areas. Figure 3(d) shows the trip demand profiles of the five boroughs of NYC. We set the ride-share service level at $\beta = 95\%$ (our main findings are robust to reasonable variations of β). Note that, in practice, this service level can be replaced with alternative service performance metrics concerning, e.g., the total or the maximum number of unsatisfied rides or unsatisfied travel distance.

In addition to taxis, ride-hailing companies (e.g. Uber and Lyft) continue to gain market share for ride-share services in NYC. Though we are unable to obtain detailed trip data from those companies, the report by TLC (2017) indicates that Uber and Lyft provided nearly 300,000 and 70,000 trips respectively per day in July 2016, while the average number of yellow and green taxi trips was 370,000 per day. Therefore, we magnify the taxi trips data by a factor of two to estimate the ride-share trip demands between any two areas.

We calibrate the travelling time, trip distances between areas and within any area based on the TLC trip record data and the geographic information. 1) All areas have within-area trips and most areas have many ride-share trips between each pair of them. We use the mean value of the data as the travelling distance d_{ij} between two areas or within one area. 2) For several pairs of areas with no data of taxi trips between them, we use a simple extrapolation to estimate the trip distance. Specifically, we calculate the straight-line distance between any two centroids i and j in Figure 2(c) and denote it by $\hat{d}_{ij}$. For areas for which the distances d are available from the data, the average ratio of d to $\hat{d}$ is a constant θ. Then we use the product

$\theta\hat{d}$ to approximate the travelling distance between the areas with no distance data available. 3) Based on the trip data, we can also calculate the travelling time $\hat{\tau}_{ijt}$ in period t by the formula $\hat{\tau}_{ijt} = d_{ij}/v_{ijt}$, in which v_{ijt} is the average driving speed for trips from area i to area j in period t and also used for calculating the per-km SOC drop. Here τ_{ij} denotes the mean value of the travelling time over all periods, i.e., $\tau_{ij} = \sum_t \hat{\tau}_{ijt}/96$. We round the the travelling time to the nearest integer.

Vehicle related parameters: Battery energy capacity and charge and discharge rates vary by vehicle models. At present, the battery capacity of a Tesla Model X 100D & P100D can be up to 100kWh, whereas most of other EV models have a capacity that ranges from 16kWh to 60kWh (Clipper Creek 2018). In this work, we set the battery capacity at 48kWh, and the charge and discharge rates at 12kW and 15kW, respectively. Both the charge and discharge conversion efficiencies are $\eta^+ = \eta^- = 90\%$. In addition, we assume that the minimum SOC and maximum SOC of an SAEV in service are $\underline{e} = 20\%$ and $\bar{e} = 100\%$, respectively. We compute the per-km energy consumption for serving customers and repositioning based on an empirical formula. In addition, if $e + d_{ij}a^s$, $e + d_{ij}a^r$, $e - \sigma^+$ or $e + \sigma^-$ is not in E, we round up the value to the nearest integer.

Regarding the per-km SOC drop due to ride-share (denoted by a^s) and repositioning (denoted by a^r), the main influencing factors include driving speed, use of onboard auxiliaries, road conditions, etc., according to Brito et al. (2013) and Badin et al. (2013). Whereas SAEVs being repositioned are vacant, passengers on ride-share trips consume extra energy by using onboard equipment. Therefore, we set $a^s > a^r = 0.8a^s$. Furthermore, to take spatially and temporally varying road traffic conditions into account, we utilize the formula $\left(a^s_{ijt} \approx (8.33e-6)v^2_{ijt} + (1.67e-4)v_{ijt} + 0.06\right)$ from Brito et al. (2013) to determine the energy drop a^s_{ijt} (in kWh/km) for trips from location i to j in period t, and assign the mean value of all ride-share trips to a^s.

Finally, assume that charge and discharge spots that are available for SAEVs account for 40% of all parking spots as estimated in a survey (Bursa 2014). Then we assume that the number of available spots in each microgrid-delimited area is proportional to its area.

Appendix D: N-1 Resilience-Constrained Fleet Dispatch Problem

Here we formulate the N-1 resilience-constrained fleet dispatch problem. Consider the normal operating condition (indexed by superscript 0) and a set of contingencies denoted by $C = \{1, 2, ..., |C|\}$. Each contingency $c \in C$ represents an event that one of the N pivotal microgrid areas, i^c, gets disconnected at period $t^c \in \hat{T}$, where $\hat{T}$

represents the set of starting hours of disruption. Here we simply set $\hat{T} = \{8\text{am}, 8\text{pm}\}$ for computational ease. Hence, the total number of contingency scenarios to consider is $|C| = N \times \left|\hat{T}\right|$. Under either the normal operating condition ($c = 0$) or a contingency ($c \in C$), we use $\mathbf{x}_t^c \equiv \{\boldsymbol{\gamma}_t^c, \boldsymbol{\rho}_t^c, \boldsymbol{\mu}_t^c, \boldsymbol{\nu}_t^c, \boldsymbol{\xi}_t^c, \boldsymbol{\zeta}_t^c, \boldsymbol{\varphi}_t^c, \boldsymbol{\psi}_t^c, \boldsymbol{\omega}_t^c, \boldsymbol{f}_t^c, \boldsymbol{h}_t^c, \boldsymbol{s}_t^c, \boldsymbol{z}_t^c\}$ to succinctly summarize all the decision variables of period t concerning SAEV-microgrid operations (i.e., ride-sharing, repositioning, charging, discharging, idling, inter-microgrid energy exchange and grid import). Let $\tau_0 = \underset{i,j \in I}{max}\{\tau_{ij}\}$, where τ_{ij} is the travel time from area i to j. To further simplify notation, let Ω^0 represent the solution space for the normal operating condition, i.e., the constraints of Problem (SS) in Subsection 4.1. Let $\Omega^c(\underline{m})$ represent the solution space under contingency $c \in C$, that is, the constraints of Problem ($\text{R}_{i^c t^c}$) in Subsection 4.2 with the modification that the minimum resilience m on the RHS of (19b) is replaced with the pre-specified level $\underline{m}$ to satisfy the N-1 criterion. Then we propose the following N-1 resilience-constrained fleet dispatch problem (RC) to be evaluated before the start of each day:

$$\begin{aligned}
\text{(RC)} \quad & \text{minimize } \Gamma((\mathbf{x}_t^0)_{t \in T_2}) \equiv \text{ Objective (18}a\text{)}, \\
& \text{subject to} \quad (\mathbf{x}_t^0)_{t \in T_2} \in \Omega^0, && (27) \\
& \qquad\qquad (\mathbf{x}_t^c)_{t \in \{t^c, \ldots, |T_2|\}} \in \Omega^c(\underline{m}), \forall c \in C, && (28) \\
& \qquad\qquad \mathbf{w}^c \left((\mathbf{x}^0_{(t^c - k)})_{k \in \{1, \ldots, \tau_0\}}, \mathbf{x}^c_{t^c}\right) = \mathbf{0}, \forall c \in C. && (29)
\end{aligned}$$

The objective is the same as defined in (18a) under the normal operating condition. The horizon is the next two days, i.e. $T_2 = \{1, ..., 192\}$, so as to contain any 12-hour contingency period following a disruption from the first 24 hours. Constraints (27) and (28) ensure that the fleet dispatch schemes under the normal operating condition and the contingencies are feasible, respectively, with the N-1 criterion satisfied. Constraint (29) represents the array of constraints that couple the system states before and after each contingency c (i.e., constraints (5), (8), (9), (12) and (13)). In other words, constraint (29) ensures feasible switching from the normal dispatch in period $t^c - k (k \in \{1, ..., \tau_0\})$ to the adjusted dispatch in period t^c under each contingency.

Note that such an N-1 resilience-constrained fleet dispatch modeling framework can be extended to evaluate the SAEV potential for improving microgrid resilience under other grid contingencies, such as a sudden drop in PV power output due to weather conditions or simultaneous disconnections in multiple areas. We leave out detailed analysis for brevity. Also note that there are other decision-making frameworks to tackle uncertain supply disruptions in the literature of supply chain design and management. For example, Gao et al. (2019) develop a distributionally robust model to optimize inventory allocation under the worst-case

CVaR performance of lost sales during disruption, characterized by a copositive program. They also present stochastic programming approaches as benchmarks. Nevertheless, we propose this N-1 criterion to highlight the long-standing risk-averse attitude of grid operators, which we will discuss in Appendix E.

Appendix E: The Conservativeness of the N-1 Criterion

We have proposed the N-1 criterion and the N-1 resilience-constrained fleet dispatch problem in Subsection 4.3. The N-1 criterion highlights the long-standing risk-averse attitude of power grid operators. To further help the reader appreciate how this N-1 approach captures uncertain failures in a deterministic and conservative fashion, in this appendix, we explain the N-1 criterion using a simple network flow example (which is simpler and more familiar to operations management readers). In what follows, we first introduce a simplified historical case study on the Soviet railway network from Alderson et al. (2014). Then we describe three flow models, namely, a basic model, a two-stage robust optimization model and an N-1 optimization model. We will show that the N-1 optimization framework is more conservative than the robust optimization framework. We largely adopt the notation in Alderson et al. (2014), as Table 8 summarizes.

Table 8 Notation in the Railway Network Example

Indices and Sets	
$k, i, j \in V$	Stations (ordered set of nodes).
$s, t \in V$	Distinguished start and end stations.
$[i, j] \in H$	Undirected edge between nodes i and j, representing the railway track from station i to j, $i < j (\forall [i, j] \in H)$.
$(i, j) \in A$	Directed arc from i to j.
C	Set of contingency scenarios, $\lvert C \rvert = \lvert H \rvert$.
Parameters	
$\underline{y}$	Pre-specified lower bound of total flow in contingency scenarios.
u_{ij}	Basic capacity limit on track $[i, j]$.
r_{ij}	Unit cost for reinforced capacity $w_{ij}, [i, j] \in H$.
x^c_{ij}	$= 1$ if track $[i, j] \in H$ is interdicted in contingency $c \in C$; $= 0$ otherwise.
Decisions	
$y_{ij} (y^c_{ij})$	Directional flow of cargo on arc $(i, j) \in A$ (in scenario c).
w_{ij}	Reinforced capacity for track $[i, j] \in H$.
x_{ij}	$= 1$ if track $[i, j] \in H$ is interdicted; $= 0$, otherwise.

Figure 1 depicts the graph $G = (V, A, u, s, t)$ that represents the railway cargo delivery system. Number pairs (u_{ij}, r_{ij}) are marked on the edges. In analogy to our baseline "no-synergy" SAEV fleet dispatch model

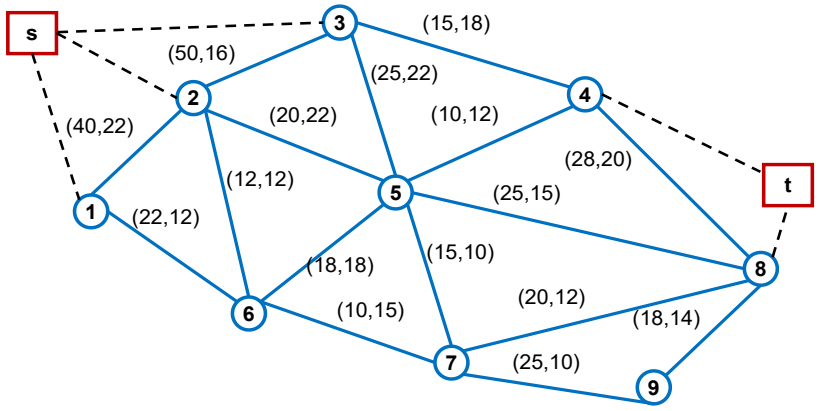

Figure 1 **A diagram of a railway network system.**

introduced in Subsection 5.2, the basic maximum flow model (Rail-Basic) can be expressed as follows (from Alderson et al. (2014)):

$$\text{(Rail-Basic)} \quad \max \ y_{ts} \tag{30}$$

$$\text{s.t.} \quad y_{ij} + y_{ji} \le u_{ij}, \forall (i,j) \in A, \tag{31}$$

$$\sum_{j:(k,j)\in A} y_{kj} - \sum_{i:(i,k)\in A} y_{ik} = \begin{cases} y_{ts} & k = s, \\ 0 & k \neq s,t, \forall k \in V, \\ -y_{ts} & k = t, \end{cases} \tag{32}$$

$$y_{ts} \ge 0, \tag{33}$$

$$y_{ij} \ge 0, \forall (i,j) \in A. \tag{34}$$

In this basic scenario, the objective (30) of the operator is to maximize the amount of cargo flowing from the start station to the destination station, subject to the capacity limit (31) of each arc and the flow balance equation (32) at each node. Constraints (33) and (34) impose non-negativity of railway flows.

Model (Rail-Basic) provides dispatch decisions for normal operations. However, resilience under contingencies is also important for critical infrastructure, such as railways, power systems and so on. The operator needs to develop proactive strategies to help maintain a secure and resilient system. For the railway network system, we consider a resilience-constrained planning and dispatch problem in analogy to the one considered for the SAEV-microgrid network in our main text. Specifically, the goal is to devise a cost-effective railway reinforcement plan such that a pre-specified railway throughput level is guaranteed after an interdiction

of a track segment (e.g., an attack on an arc). Let the binary variable $x_{ij} = 1$ indicate that track $[i, j]$ is interdicted so that the capacity on the track is reduced to zero and not available for carrying cargo. We consider the following two modeling frameworks to capture the uncertainty of the interdiction location.

First, the *two-stage robust optimization model* aims to identify the worst-case contingency in the second stage and accordingly make infrastructure reinforcement plan in the first stage. The worst-case contingency is equivalent to the event that an attacker, in anticipation of the operator's corrective re-dispatch, interdicts a single track so as to reduce the total network flow to the greatest extent. The formulation is as follows (as a modified version of the interdiction model in Alderson et al. (2014)):

$$\text{(Rail-RO)} \quad \min_{w} \sum_{[i,j]\in H} r_{ij} w_{ij} \tag{35}$$

$$\text{s.t.} \quad \min_{x} \max_{y} \quad y_{ts} \geq \underline{y}, \tag{36}$$

$$\sum_{[i,j]\in H} x_{ij} = 1, \tag{37}$$

$$y_{ij} + y_{ji} \leq (1 - x_{ij})(u_{ij} + w_{ij}), \forall [i, j] \in H, \tag{38}$$

$$\text{Constraints (32)-(34).}$$

The objective (35) of the operator is to minimize the reinforcement cost for expanding capacity on the tracks in preparation for a single attack (constraint (37)). Constraint (36) ensures the pre-specified total network flow $\underline{y}$ even under the worst attack. Constraint (38) sets the capacity limit on each track.

Second, the *N-1 optimization model* considers $N = |H| = |C|$ contingencies. Each contingency involves one track $[i, j] \in H$ interdicted and the other $|H| - 1$ tracks operating normally. The N-1 criterion specifies that, to ensure the resilience of the railway network system, the operator wants to make reinforcement investment to maintain the pre-specified flow level $\underline{y}$ no matter which one of the $|H|$ tracks is interdicted. The formulation is given as follows:

$$\text{(Rail-N-1)} \quad \min_{w} \sum_{[i,j]\in H} r_{ij} w_{ij} \tag{39}$$

$$\text{s.t.} \quad \max_{y^c} \quad y^c_{ts} \geq \underline{y}, \forall c \in C, \tag{40}$$

$$y^c_{ij} + y^c_{ji} \leq (1 - x^c_{ij})(u_{ij} + w_{ij}), \forall [i, j] \in H, \tag{41}$$

$$\sum_{j:(k,j)\in A} y_{kj}^c - \sum_{i:(i,k)\in A} y_{ik}^c = \begin{cases} y_{ts}^c & k=s, \forall c \in C, \\ 0 & k \neq s,t, \forall k \in V, \forall c \in C, \\ -y_{ts}^c & k=t, \forall c \in C, \end{cases} \tag{42}$$

$$y_{ij}^c \geq 0, \forall (i,j) \in A, \forall c \in C, \tag{43}$$

$$y_{ts}^c \geq 0, \forall c \in C. \tag{44}$$

The above $N-1$ resilience-constrained model comprises $|H|+1$ blocks. The objective (39) is to minimize the reinforcement investment considering $|H|$ scenarios. Constraint (40) sets the lower bound for total network flow under each scenario. Constraints (41)-(44) specify flow balance, capacity limits and variable nonnegativity under each scenario.

Comparing the two-stage robust optimization model (Rail-RO) and the N-1 optimization model (Rail-N-1) shows that the latter is more conservative than the former. In other words, the optimal reinforcement cost given by (Rail-N-1) is the upper bound for that given by (Rail-RO). This is because (Rail-RO) only considers the worst-case scenario, whereas (Rail-N-1) takes all the contingency scenarios into account. Hence, the feasible region of (Rail-RO) contains that of (Rail-N-1). Any feasible reinforcement investment decision that satisfies (Rail-N-1) thus also satisfies (Rail-RO). Therefore, the optimal objective value of (Rail-N-1) is no smaller than that of (Rail-RO).

The above discussion highlights the conservativeness of the N-1 approach. Although the N-1 criterion is not common in the operations management literature, it is common in the context of power system planning and operations. We develop the N-1 resilience-constrained model in Appendix D to highlight that the risk attitudes of different system operators differ from each other when those systems interface each other for joint smart city operations.

Appendix F: Computational Details

The SAEV fleet dispatch problem (SS) is of high dimension (e.g., involving 1,004,160 variables and 431,233 constraints in our numerical case I.c in Subsection 5.2. The optimization model can be implemented in a rolling-horizon framework (e.g., every 15 minutes). When the decision-makers get the updated information about solar radiation intensity, load profiles or travelling demands, the model can be solved again to obtain real-time operational decisions for SAEVs and microgrids. The problem can be readily reformulated as a linear program to ensure computational tractability. All the computational tests are ran on Ubuntu server

with Intel(R) Xeon(R) processor and 32GB RAM, and solved by Gurobi within minutes (e.g., the average computational time for solving the SAEV fleet dispatch problem (SS) under the full-support scenario is less than four minutes). The weighted-objective formulation also allows us to analyze the tradeoffs of the SAEV-microgrid system in Section 5. On the other hand, we choose not to incorporate some other factors: For example, for the scope of this paper, we do not extend the model to study location-based electricity pricing that can be used to induce optimal participation of private EV operating entities. We do not explicitly consider short-term fluctuations of PV output and the uncertainties of ride-share demands and travel times, which have insignificant impact on the metrics considered in our model. The impact of major interruption of PV generation due to unforeseen weather conditions can be inferred from our subsequent analysis of microgrid resilience. Finally, we assume that power flows due to demand-response executions, combined heat and power generation, and charge/discharge of non-dispatchable private EVs are all consolidated into the local aggregate demand profiles. Although these demand-side energy resources may be present in microgrids, they are peripheral to our focus on the synergy between SAEVs and solar-powered microgrids.

Appendix G: Financial and Emission Implications

For the microgrids considered in our NYC setting, what are the investment costs and carbon emissions implications of the grid assets, namely the PV solar panels, the energy storage devices and the SAEVs? We next provide those estimates (costs are presented in 2020 dollars adjusting for inflation of 2.5% per year).

Investment Costs. Begin with the investments in PV panels. The cost of PV panels is $\$4.10 - \$10.25$ per square foot (Homeguide 2019). We thus set \$37.46 per square meter as the average projected value in 2030 considering the cost reduction of 51.49% over 2020-2030 (IRENA 2019). Given an average lifetime of 30 years (IRENA and IEA-PVPS 2016), the 30% PV adoption level considered in our setting translates to nearly 38.87 million square meters of PV panels, meaning an investment of \$0.13 million per day.

As for energy storage in 2030, the cost projection for lithium-ion systems is \$218.53/kWh according to (Cole and Frazier 2020) with a life expectancy of 10 years (NYSDPS 2018). Therefore, our setting with 5GWh storage capacity amounts to a total investment of \$0.30 million per day.

In 2030, each SAEV will cost $\$42,645$ (BCG 2017) with an average life span of 8 years (Krishnan 2018), whereas each internal combustion engine (ICE) vehicle lasting for 10 years (Arbin Instruments 2020) will cost $\$33,114$ (Soulopoulos 2017). Subsequently, the investments in the small fleet with 80,000 SAEVs and the large fleet with 500,000 SAEVs are \$1.17 million and \$7.30 million per day, respectively. Collectively,

the total investment in the PV panels, the energy storage devices and the small-sized SAEV fleet is \$1.60 million per day in our setting.

Carbon Emissions. We next estimate carbon emissions with different combinations of PV panels, energy storage devices and SAEVs in the city. Non-renewable power generation and ICE vehicles are responsible for carbon emissions. For the transportation sector, the emission factor of gasoline is 8.78 kg CO_2 per gallon (EPA 2018a), and the average fuel economy is 22 miles per gallon (EPA 2018b). For grid import, the amount of carbon emissions is related to the energy mix of electricity generation. In line with the New York state's goal of sourcing 70% of its electricity from renewable energy by 2030 (John 2020), we assume that the remaining 30% electricity is mainly generated by natural gas. One cubic feet natural gas can generate 0.10 kWh electricity (Statista 2016) and emit 54.44g CO_2 (EPA 2018a).

With these estimates, consider a baseline scenario in which only ICE vehicles satisfy travelling demands, and the entire city is 100% powered by the external grid. The total carbon emissions in this baseline is 32,986 ton per day. However, this value can be reduced by 45.37% if assuming the 30% PV adoption level in our numerical setting. Further adding energy storage devices and the small-sized SAEV fleet can bring another 4.21% of emission savings. In addition, assume the social cost of carbon to be \$0.069 per kilogram in 2030 (with a 3% discount rate, EPA (2016)). Then the total social cost of carbon emissions implied by our setting is 1.15 million per day.

Energy storage and SAEVs are mutually substitutable for saving emissions. At the 30% PV adoption level, the small-sized SAEV fleet is equivalent to 5.23 GWh of energy storage for achieving a 47.44% saving of carbon emissions relative to the above baseline scenario. Our numerical tests also show that the marginal emission-saving effect diminishes to zero as the SAEV fleet size becomes more than 1.07 million (achieving a 57.47% emission saving) or the storage capacity becomes over 40 GWh (achieving a 54.92% emission saving).

The facts that the total investment cost of SAEVs far exceeds that of energy storage and that energy storage can substitute SAEVs for grid support and emission saving may suggest that the city should fully displace SAEVs with energy storage. However, the adoption of SAEVs is mainly driven by the urban mobility needs. The prevalence of SAEVs may potentially avoid extra investment in stationary energy storage that otherwise would have to be installed. It will be worth investigating the optimal mix of stationary energy storage and SAEVs in future studies.

References

8MSolar (2016) What is a Peak-Sun Hour (PSH)? https://www.8msolar.com/what-is-a-peak-sun-hour-psh.

Alderson D, Brown G, Carlyle W (2014) Assessing and improving operational resilience of critical infrastructures and other systems. *Tutorials in Operations Research: Bridging Data and Decision.San Francisco,CA, USA: INFORMS* 180–215.

Arbin Instruments (2020) Game-changing million mile electric vehicle battery. https://www.arbin.com/tag/calt/.

Badin F, Le Berr F, Briki H, et al (2013) Evaluation of EVs energy consumption influencing factors, driving conditions, auxiliaries use, driver's aggressiveness. *World Electric Vehicle Journal* 112–123.

Battery University (2018) BU-1003: Electric Vehicle (EV). http://batteryuniversity.com/learn/article/electric_vehicle_ev.

BCG (2017) Reimagined car: Shared, autonomous, and electric vehicle. https://www.bcg.com/en-ca/publications/2017/reimagined-car-shared-autonomous-electric.aspx.

Brito F, Martins J, et al (2013) *Real-Life Comparison Between Diesel and Electric Car Energy Consumption, in Grid Electrified Vehicles: Performance, Design and Environmental Impacts.* (Nova Science Publishers).

Bursa J (2014) Counting New York's parking spots. http://zamez.org/articles/nyc-parking-data.

Clipper Creek (2018) How long does it take to charge an electric car? https://www.clippercreek.com/charging-times-chart/.

Cole W, Frazier A (2020) End-of-life management: solar photovoltaic panels. Technical report, National Renewable Energy Lab (NREL), Golden, CO (United States).

Department of City Planning (2018) PLUTO data set. https://www1.nyc.gov/site/planning/data-maps/open-data/bytes-archive.page?sorts[year]=0.

EERE (2014) Commercial and residential hourly load profiles for all TMY3 locations in the United States. https://openei.org/datasets/dataset/commercial-and-residential-hourly-load-profiles-for-all-tmy3-locations-in-the-united-states.

EPA (2016) EPA fact sheet-social cost of carbon. https://www.epa.gov/sites/production/files/2016-12/documents/social_cost_of_carbon_fact_sheet.pdf.

EPA (2018a) Emission factors for greenhouse gas inventories. https://www.epa.gov/sites/production/files/2018-03/documents/emission-factors_mar_2018_0.pdf.

EPA (2018b) Greenhouse gas emissions from a typical passenger vehicle. Technical report, United States Environmental Protection Agency.

Gao SY, Simchi-Levi D, Teo CP, Yan Z (2019) Disruption risk mitigation in supply chains: The risk exposure index revisited. *Operations Research* 67(3):831–852.

Homeguide (2019) How much do solar panels cost? https://homeguide.com/costs/solar-panel-cost.

IRENA (2019) Future of solar photovoltaic: Deployment, investment, technology, grid integration and socio-economic aspects (a global energy transformation: paper). Technical report, International Renewable Energy Agency, Abu Dhabi.

IRENA, IEA-PVPS (2016) End-of-life management: solar photovoltaic panels. Technical report, International Renewable Energy Agency and International Energy Agency Photovoltaic Power Systems.

John JS (2020) New Yorks energy transition (and challenges) in 5 Charts. https://www.greentechmedia.com/articles/read/the-challenges-of-greening-new-yorks-power-grid.

Krishnan S (2018) Electric car parts life expectancy: How long an EV lasts? https://getelectricvehicle.com/electric-car-parts-life-expectancy-how-long-an-ev-lasts/.

NREL (2014) National solar radiation database 1998-2014 update (National Renewable Energy Laboratory). http://rredc.nrel.gov/solar/old_data/nsrdb/.

NYISO (2018) Load data. http://www.nyiso.com/public/markets_operations/market_data/load_data/index.jsp.

NYSDPS (2018) New York State energy storage roadmap and Department of Public Service/New York State energy research and development authority staff recommendations. Technical report, Department of Public Service, New York.

NYSERDA (2018) Electricity sales by sector, GWh: Beginning 1980. https://data.ny.gov/Energy-Environment/Electricity-Sales-By-Sector-GWh-Beginning-1980/pv7j-5nz8.

Pepco (2020) Criteria limits for distributed energy resource connections to the ACE, DPL and Pepco distribution systems (less than 69kv). https://www.pepco.com/MyAccount/MyService/Pages/CriteriaSummary.aspx.

Pickerel K (2020) Navigant Research expects lithium-ion batteries to make up 85% of newly installed storage capacity this year. https://www.solarpowerworldonline.com/2020/03/navigant-research-expects-lithium-ion-batteries-to-make-up-85-of-newly-installed-storage-capacity-this-year/.

Soulopoulos N (2017) When will electric vehicles be cheaper than conventional vehicles? Technical report, Bloomberg New Energy Finance (BNEF).

Statista (2016) How much electricity is generated from a unit of coal, natural gas and oil in the U.S. ? https://www.statista.com/statistics/216613/electricity-generated-per-unit-of-fuel-used/#statisticContainer.

TLC (2017) TLC trip record data NYC. www.nyc.gov/html/tlc/html/about/trip_record_data.shtml.

Ward T (2017) This is the most efficient solar panel ever made. https://www.weforum.org/agenda/2017/08/this-is-the-most-efficient-solar-panel-ever-made.

Zablocki A (2019) Fact sheet: Energy storage (2019). https://www.eesi.org/papers/view/energy-storage-2019.